Supporting Information

Exploring the Relationship between Effective Mass, Transient Photoconductivity, and Photocatalytic Activity of $Sr_xPb_{1-x}BiO_2Cl$ (x = 0–1) Oxyhalides

Hajime Suzuki,[†,‡] Shohei Kanno,[§] Masahiko Hada,[§] Ryu Abe,[*,‡,ǁ] and Akinori Saeki[*,†,⊥]

[†]Department of Applied Chemistry, Graduate School of Engineering, Osaka University, 2-1 Yamadaoka, Suita, Osaka 565-0871, Japan
[‡]Department of Energy and Hydrocarbon Chemistry, Graduate School of Engineering, Kyoto University, Katsura, Nishikyo-ku, Kyoto 615-8510, Japan
[§]Department of Chemistry, Tokyo Metropolitan University, Hachioji, Tokyo 192-0364, Japan
[ǁ]CREST, Japan Science and Technology Agency (JST), Kawaguchi, Saitama 332-0012, Japan
[⊥] Precursory Research for Embryonic Science and Technology (PRESTO), Japan Science and Technology Agency (JST), 4-1-8 Honcho, Kawaguchi, Saitama 332-0012, Japan

AUTHOR INFORMATION
Corresponding Author
* ryu-abe@scl.kyoto-u.ac.jp (R. A.); saeki@chem.eng.osaka-u.ac.jp (A. S.)

This supporting information presents the following contents.

Methods
Supporting References
Supporting Tables S1-S5
Supporting Figures S1-S15

Methods

Computational details

All periodic boundary condition (PBC) calculations were performed using Perdew–Burke–Ernzerhof (PBE) exchange correlation functional with projector augmented wave (PAW) pseudopotentials, and 600 eV plane-wave cut-off in Vienna ab initio simulation package (VASP) code.[S1–S7] Note that the use of Heyd-Scuseria-Ernzerhof hybrid functional (HSE06), [S8] instead of PBE, leads to a small difference in the band dispersion. In order to determine the atomic orbital energies of constituent elements in $PbBiO_2Cl$ and $SrBiO_2Cl$, *ab initio* atomic orbital calculations were carried out. The orbital energies were estimated by the SOC approach with relativistic Hamiltonian based on ZORA with the PBE exchange correlation functional,[S9, S10] as implemented in the Amsterdam density functional program package (ADF 2017). [S11] ZORA triple-zeta + polarized (TZP) was used as basis set.[S12]

DFT calculations were performed to compare the electron and hole effective masses in the solid solutions ($Sr_{0.25}Pb_{0.75}BiO_2Cl$, $Sr_{0.5}Pb_{0.5}BiO_2Cl$, and $Sr_{0.75}Pb_{0.25}BiO_2Cl$). The most part of the computational method is common to that for $PbBiO_2Cl$ and $SrBiO_2Cl$ which is summarized in main text. For the solid solutions, 4, 6, and 4 types of unit cells were considered for $Sr_{0.25}Pb_{0.75}BiO_2Cl$, $Sr_{0.5}Pb_{0.5}BiO_2Cl$, and $Sr_{0.75}Pb_{0.25}BiO_2Cl$ solid solutions, respectively. Because, 4 ion sites of Pb or Sr exist in the unit cell at orthorhombic phase, and the 4, 6, and 4 types of unit cells can be generated for each solid solution according the ratio of Pb and Sr. In this study, geometry optimizations of the ions and lattice constants were performed for the all types of unit cells of each solid solution. The electron and hole effective masses were calculated for the most stable structures in each solid solution. The methodology of density functional theory (DFT) calculations for the solid solutions are the same as that for $PbBiO_2Cl$ and $SrBiO_2Cl$.

Supporting References

(S1) Perdew, J. P.; Burke, K.; Ernzerhof, M. Generalized gradient approximation made simple. *Phys. Rev. Lett.* **1996**, *77*, 3865−3868.

(S2) Perdew, J. P.; Burke, K.; Ernzerhof, M. Generalized gradient approximation made simple (vol 77, pg 3865, 1996). *Phys. Rev. Lett.* **1997**, *78*, 1396−1396.

(S3) Kresse, G.; Furthmuller, J. Efficiency of ab-initio total energy calculations for metals and semiconductors using a plane-wave basis set. *Comp. Mater. Sci.* **1996**, *6*, 15−50.

(S4) Kresse, G.; Furthmuller, J. Efficient iterative schemes for ab initio total-energy calculations using a plane-wave basis set. *Phys. Rev. B* **1996**, *54*, 11169−11186.

(S5) Kresse, G.; Hafner, J. Abinitio Molecular-Dynamics for Liquid-Metals. *Phys. Rev. B* **1993**, *47*, 558−561.

(S6) Kresse, G.; Hafner, J. Ab-Initio Molecular-Dynamics Simulation of the Liquid-Metal Amorphous-Semiconductor Transition in Germanium. *Phys. Rev. B* **1994**, *49*, 14251−14269.

(S7) Kresse, G.; Joubert, D. From ultrasoft pseudopotentials to the projector augmented-wave method.

Phys. Rev. B **1999**, *59*, 1758−1775.

(S8) Krukau, A. V.; Vydrov, O. A.; Izmaylov, A. F.; Scuseria, G. E. Influence of the exchange screening parameter on the performance of screened hybrid functionals. *J. Chem. Phys.* **2006**, *125*, 224106.

(S9) Eschrig, H.; Servedio, V. D. P. Relativistic density functional approach to open shells. *J. Comput. Chem.* **1999**, *20*, 23−30.

(S10) van Wullen, C. Spin densities in two-component relativistic density functional calculations: Noncollinear versus collinear approach. *J. Comput. Chem.* **2002**, *23*, 779−785.

(S11) te Velde, G. *et al.* Chemistry with ADF. *J. Comput. Chem.* **2001**, *22*, 931−967.

(S12) Van Lenthe, E.; Baerends, E. J. Optimized slater-type basis sets for the elements 1-118. *J. Comput. Chem.* **2003**, *24*, 1142−1156.

(S13) Koopmans, T. Über die Zuordnung von Wellenfunktionen und Eigenwerten zu den Einzelnen Elektronen Eines Atoms. *Physica* **1934**, *1*, 104−113.

(S14) Petricek, V.; Dusek, M.; Palatinus, L. Crystallographic Computing System JANA2006: General features. *Z. Kristallogr.* **2014**, *229*, 345−352.

Table S1. Calculated effective masses (m_0 unit) in x, y, and z directions (m^*_{xx}, m^*_{yy}, and m^*_{zz}) and average effective masses (m^*_{avg}) of hole and electron for $Sr_xPb_{1-x}BiO_2Cl$ (x = 0.25, 0.50, 0.75).

Effective	x = 0.25		x = 0.5		x = 0.75	
mass	Electron	Hole	Electron	Hole	Electron	Hole
m^*_{xx}	0.39	3.31	0.54	1.16	0.56	1.19
m^*_{yy}	0.36	1.21	1.54	1.34	1.35	10.19
m^*_{zz}	1.66	46.48	2.49	4.02	8.57	9.36
m^*_{avg}	0.50	2.61	1.03	1.61	1.14	2.87

Table S2. Lattice constants and volumes of $Sr_xPb_{1-x}BiO_2Cl$.

x	a (Å)	b (Å)	c (Å)	V (Å^3)
0	5.5797(17)	5.5803(19)	12.4054(2)	386.26(14)
0.02	5.5799(3)	5.5816(3)	12.4137(2)	386.62(14)
0.05	5.5780(18)	5.5803(18)	12.4131(19)	386.38(13)
0.1	5.5806(4)	5.5822(4)	12.4250(2)	387.06(15)
0.15	5.5823(4)	5.5837(4)	12.4366(2)	387.64(14)
0.2	5.5866(3)	5.5881(3)	12.4556(2)	388.84(15)
0.3	5.5893(5)	5.5904(5)	12.4822(4)	390.03(2)
0.4	5.5939(5)	5.5948(4)	12.5095(5)	391.50(3)
0.5	5.603(7)	5.599(7)	12.5181(4)	392.71(3)
0.6	5.6119(5)	5.6025(5)	12.5171(4)	393.55(2)
0.8	5.6545(4)	5.5994(3)	12.4612(8)	394.54(5)
1	5.7011(2)	5.5937(2)	12.4241(7)	396.21(4)

Table S3. Calculated effective masses for a $PbBiO_2Cl$ structure with the obtained lattice constants (Table S2).

Effective mass	Model 1[a]		Model 2[b]	
	Electron	Hole	Electron	Hole
m^*_{xx}	0.28	0.94	0.29	1.13
m^*_{yy}	0.27	0.98	0.28	1.00
m^*_{zz}	0.59	8.04	0.74	5.81
m^*_{avg}	0.33	1.36	0.35	1.46

[a] The lattice constants were fixed and the ion positions are unfixed during the geometry optimization.

[b] Both the lattice constants and the ion positions are unfixed during the geometry optimization.

Table S4. Integral breadths, full width at half maxima, and crystallite sizes for (111) facet peaks in the XRD patterns of $Sr_xPb_{1-x}BiO_2Cl$.

x	Integral breadth[a] (deg.)	FWHM[a] (deg.)	Crystallite size[b] (Å)
0	0.171(4)	0.137(2)	526
0.02	0.158(3)	0.127(2)	571
0.05	0.172(3)	0.1375(18)	524
0.1	0.173(3)	0.137(2)	520
0.15	0.187(4)	0.1491(18)	482
0.2	0.176(3)	0.142(2)	511
0.3	0.181(3)	0.1449(18)	497
0.4	0.207(4)	0.1643(13)	437
0.5	0.210(4)	0.1687(16)	429
0.6	0.232(4)	0.1837(16)	388
0.8	0.275(5)	0.2169(14)	328
1	0.273(6)	0.2032(19)	330

[a]Integral breadths and full-width at the half maxima (FWHMs) were determined from the split pseudo-Voigt function fitting.

[b]Crystallite sizes were estimated by the Scherrer equation (K = 1) using the integral breadths.

Table S5. Photocatalytic O_2 evolution rate over $Sr_xPb_{1-x}BiO_2Cl$ (x = 0, 0.2) loaded with cocatalysts.

Photocatalyst	Cocatalyst[a]	O_2 evolution rate (μmol/h)
$PbBiO_2Cl$	none	12.8
$PbBiO_2Cl$	CoO_x	3.9
$PbBiO_2Cl$	IrO_x	4.2
$PbBiO_2Cl$	RuO_x	9.9
$Sr_{0.2}Pb_{0.8}BiO_2Cl$	none	6.2
$Sr_{0.2}Pb_{0.8}BiO_2Cl$	RuO_x	5.7

[a]Cocatalysts were loaded on the photocatalysts by impregnation method using corresponding precursors ($Co(NO_3)_2$, Na_2IrCl_6, $RhCl_3$: 0.5 wt% as metal), followed by calcination in air at 673 K for 30 min.

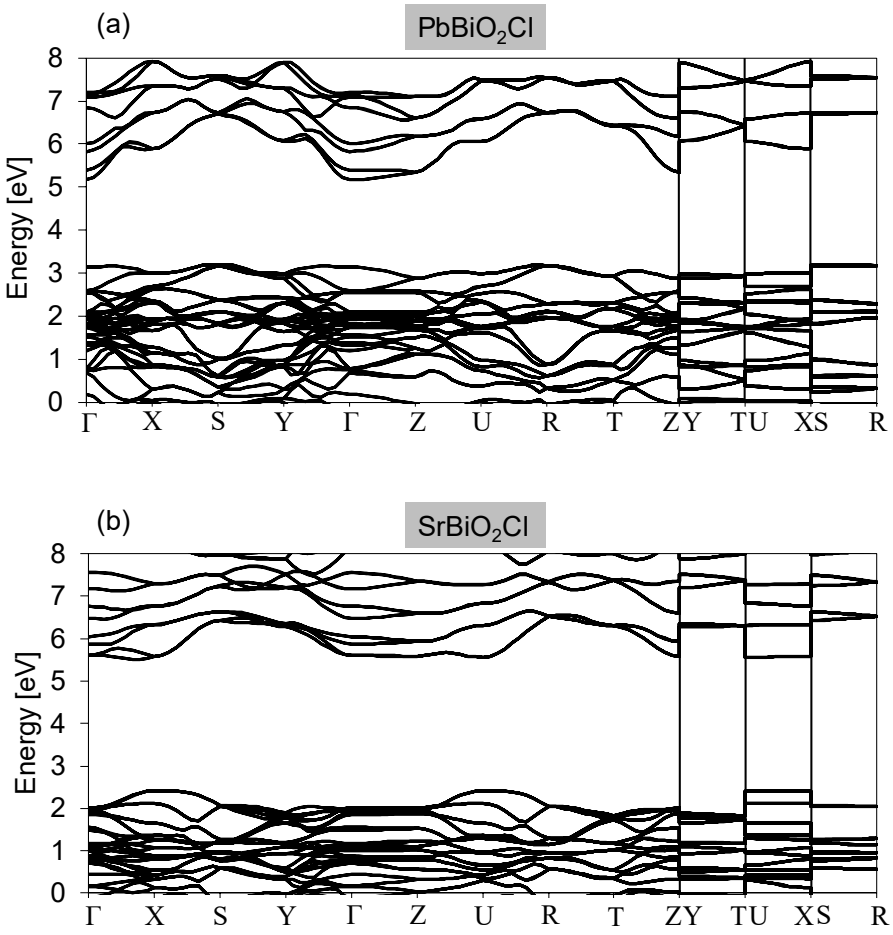

Figure S1. Band structure of (a) $PbBiO_2Cl$ and (b) $SrBiO_2Cl$.

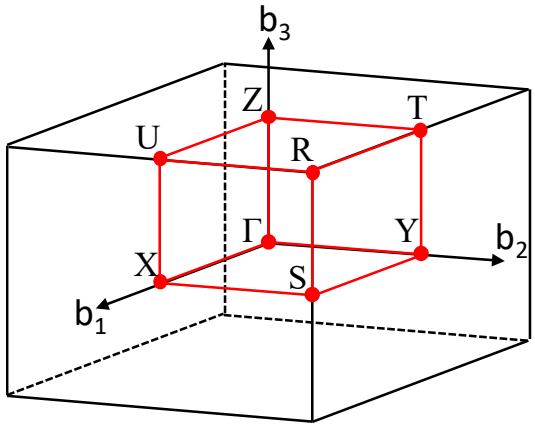

Figure S2. First Brillouin zone of orthorhombic lattice.

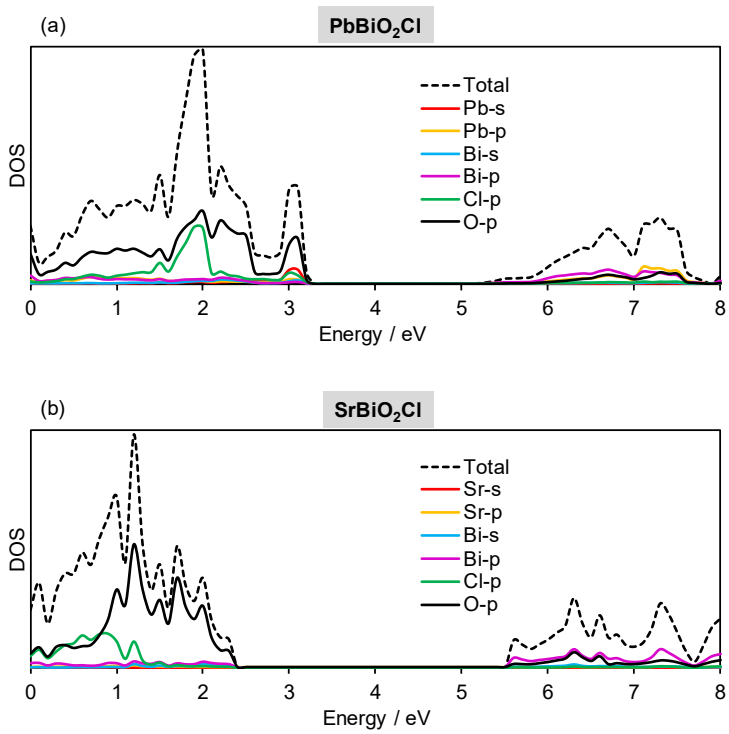

Figure S3. Full range of DOS of (a) $PbBiO_2Cl$ and (b) $SrBiO_2Cl$.

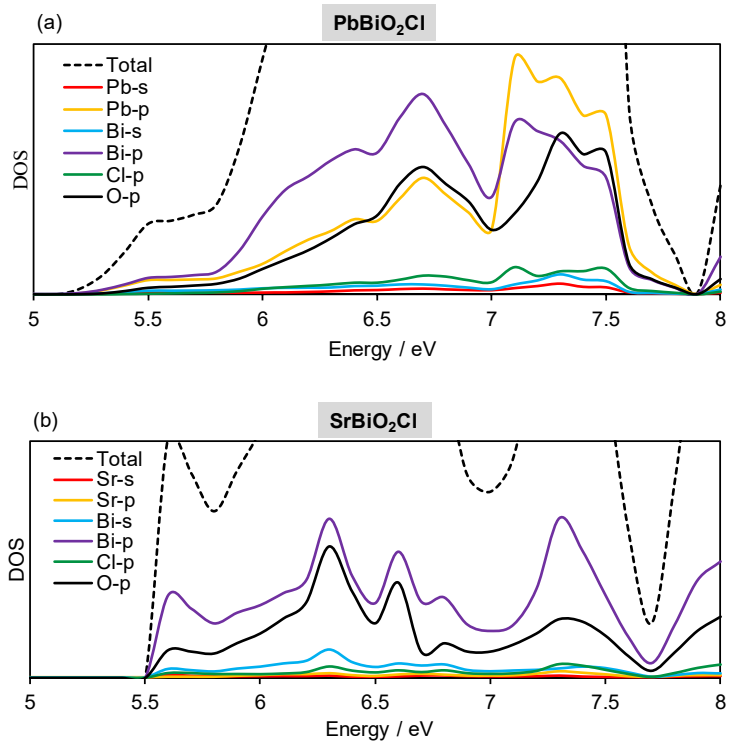

Figure S4. Magnified DOS around conduction bands of (a) $PbBiO_2Cl$ and (b) $SrBiO_2Cl$.

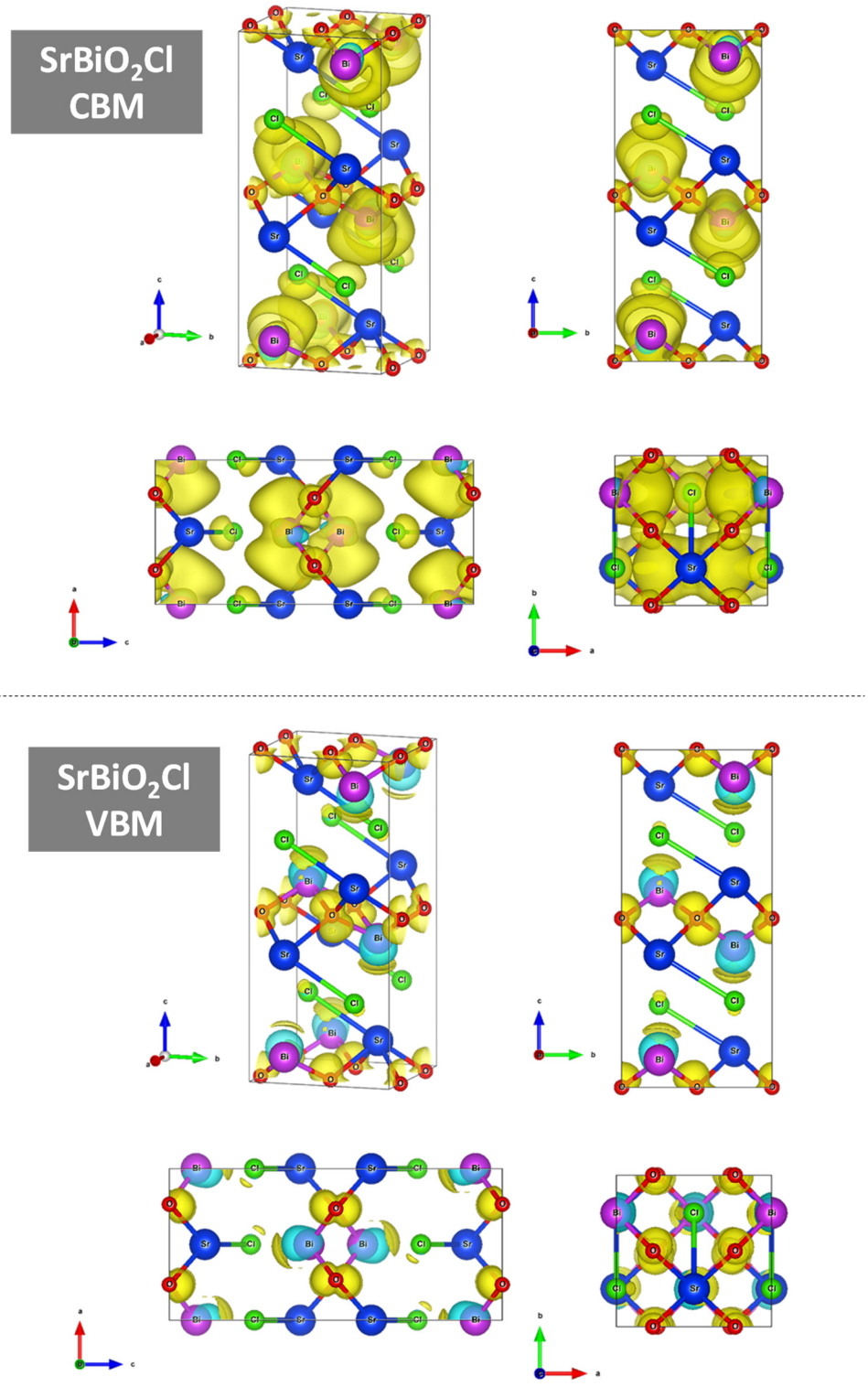

Figure S5. Partial charge densities of the CBM and VBM for $SrBiO_2Cl$. Blue, purple, red, and green spheres represent Sr, Bi, O, and Cl atoms, respectively.

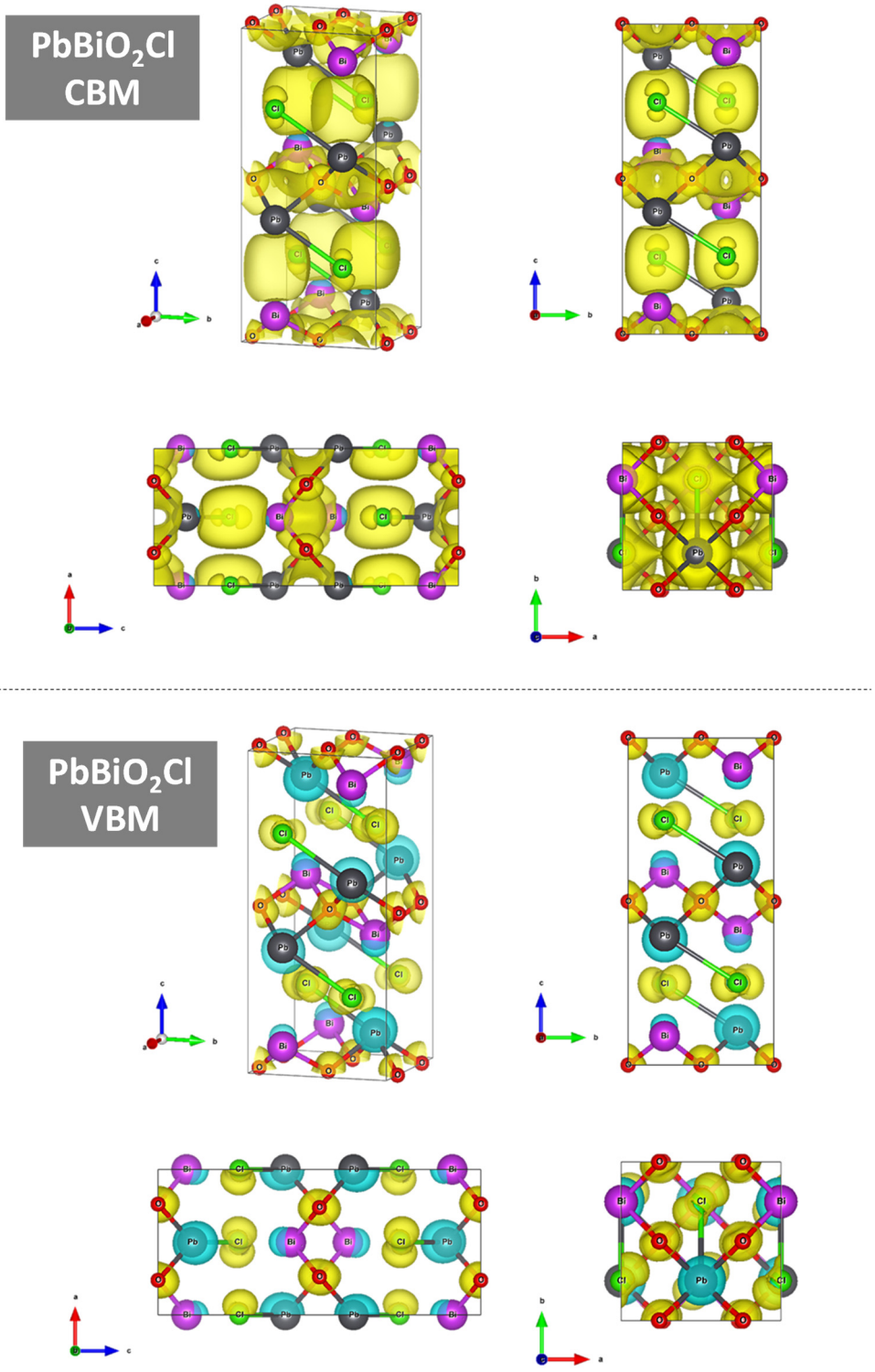

Figure S6. Partial charge densities of the CBM and VBM for $PbBiO_2Cl$. Gray, purple, red, and green spheres represent Pb, Bi, O, and Cl atoms, respectively.

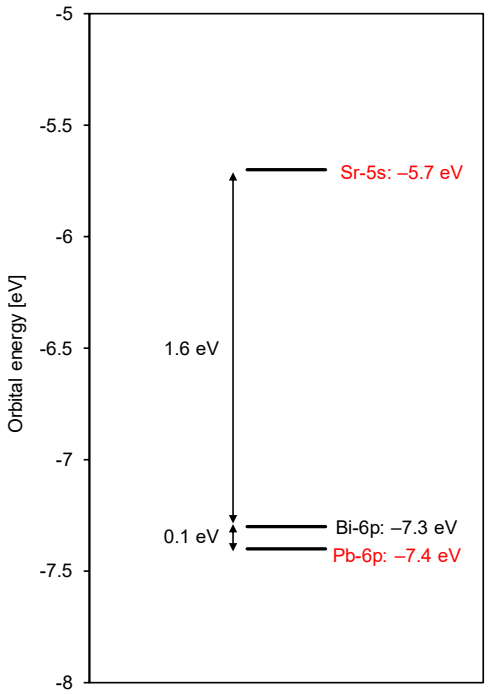

Figure S7. Orbital energies of Sr-5s, Pb-6p, and Bi-6p. The orbital energies were estimated from the first ionization potentials according to the Koopmans' theorem,[S13] because DFT calculations of these orbital energies were difficult due to the varieties of electron configuration and the electron correlations in the 6p orbitals.

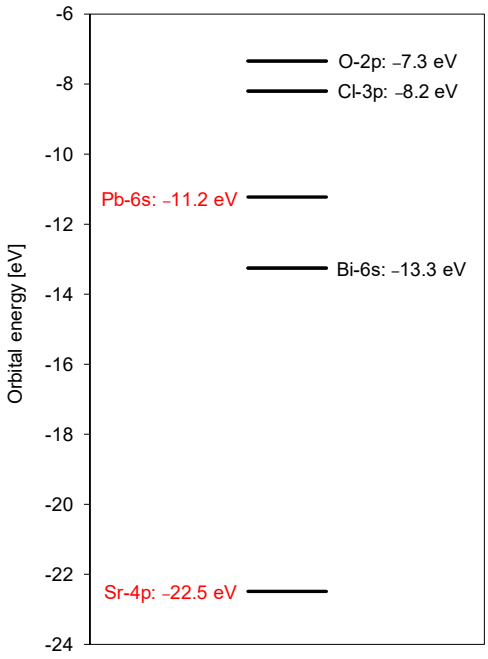

Figure S8. Orbital energies of O-2p, Cl-3p, Pb-6s, Bi-6s, and Sr-4p.

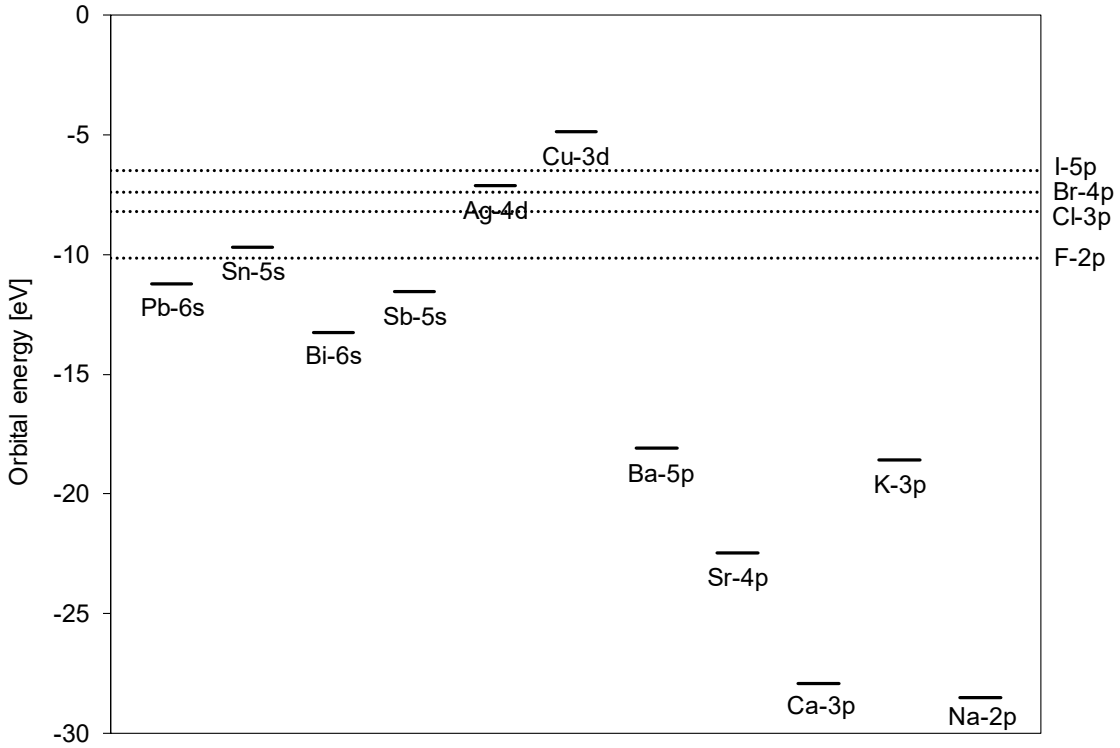

Figure S9. Various orbital energies (Pb-6s, Sn-5s, Bi-6s, Sb-5s, Ag-4d, Cu-3d, Ba-5p, Sr-4p, Ca-3p, K-3p, Na-2p). Note that the energies of d orbitals from DFT calculation generally include some imprecision due to the strong electron correlation.

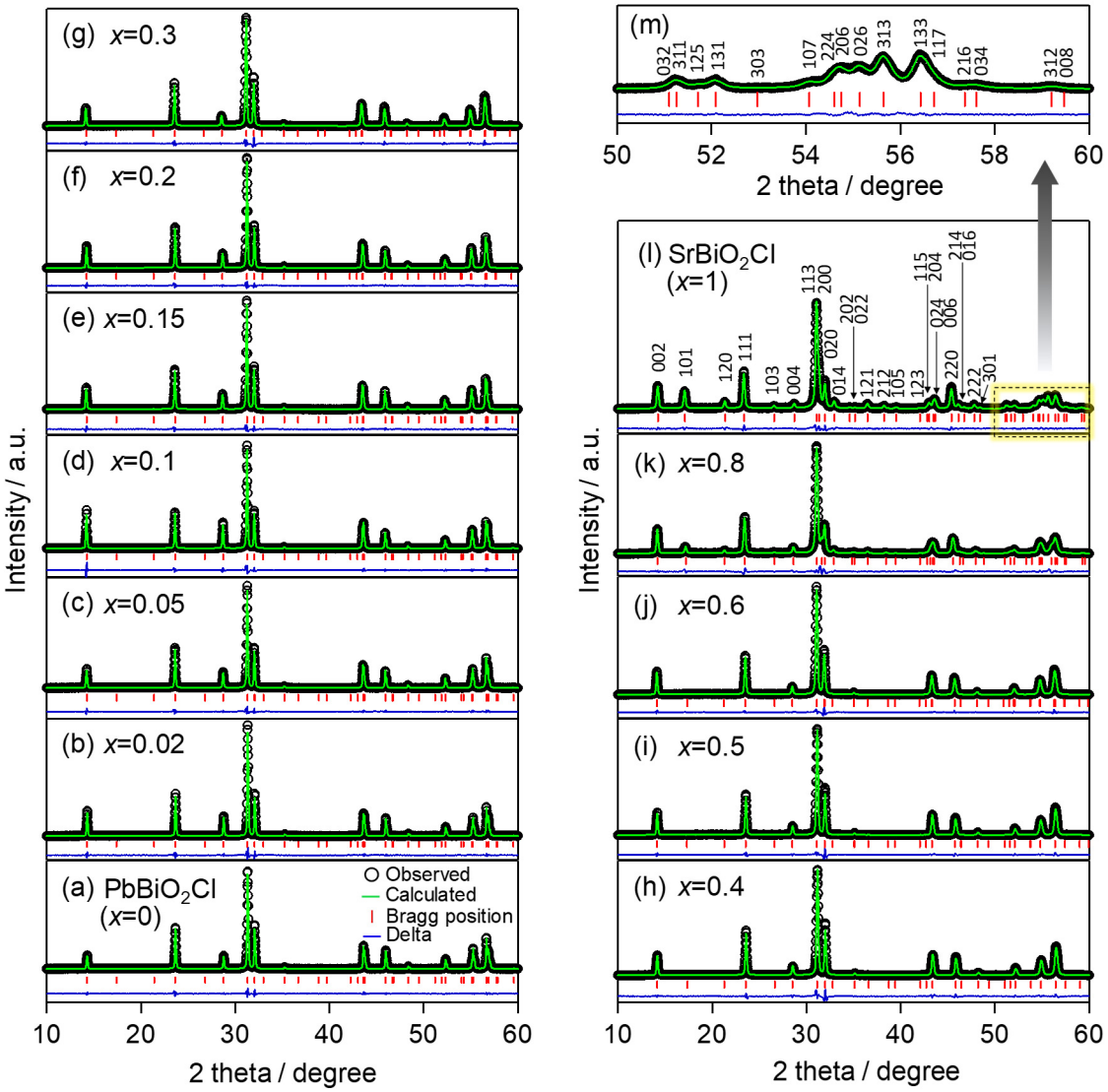

Figure S10. Le Bail refinements of XRD patterns of $Sr_xPb_{1-x}BiO_2Cl$ solid solutions using JANA 2006.[S14]

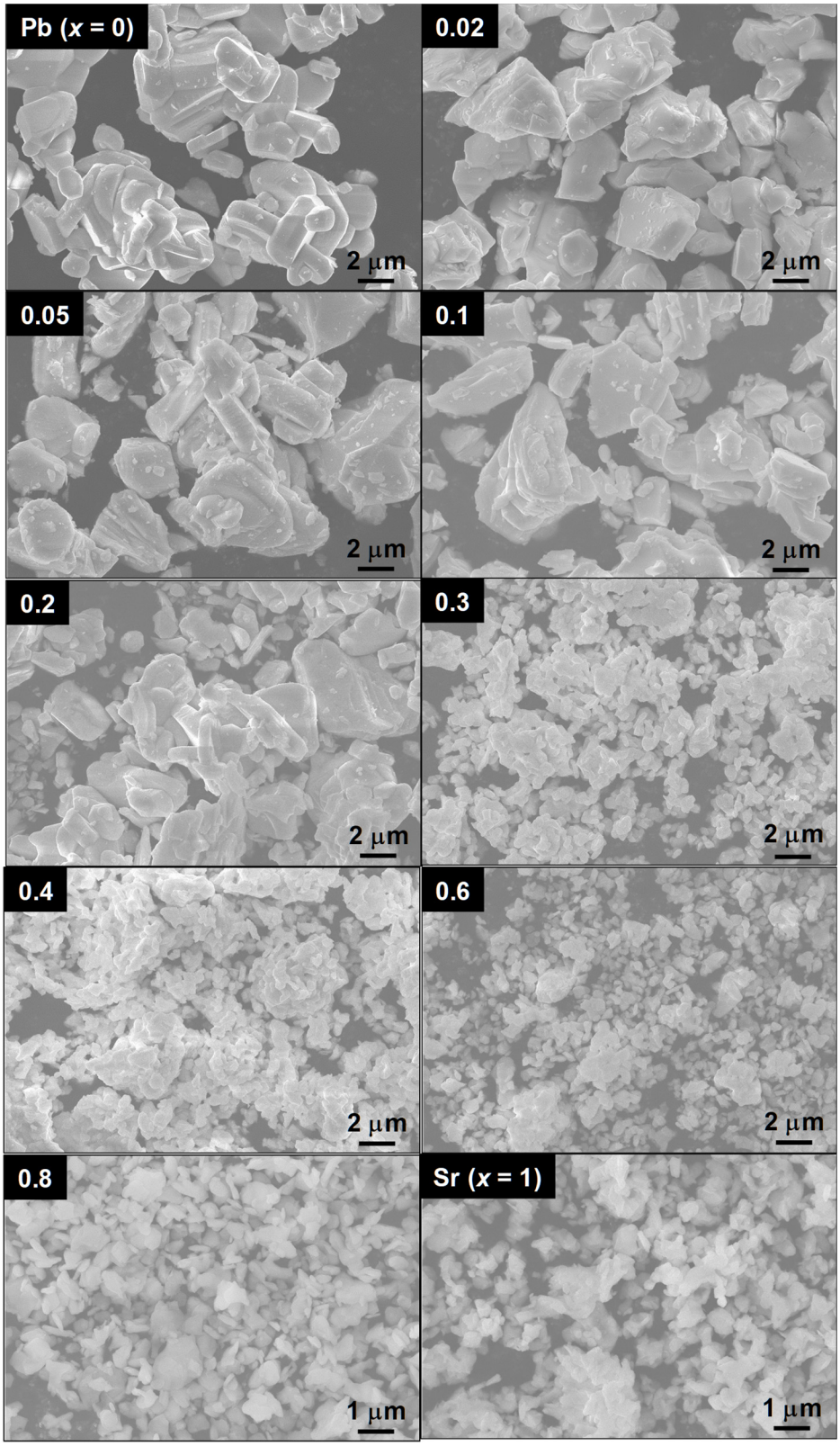

Figure S11. Enlarged SEM images of $Sr_xPb_{1-x}BiO_2Cl$ solid solutions (x = 0–1).

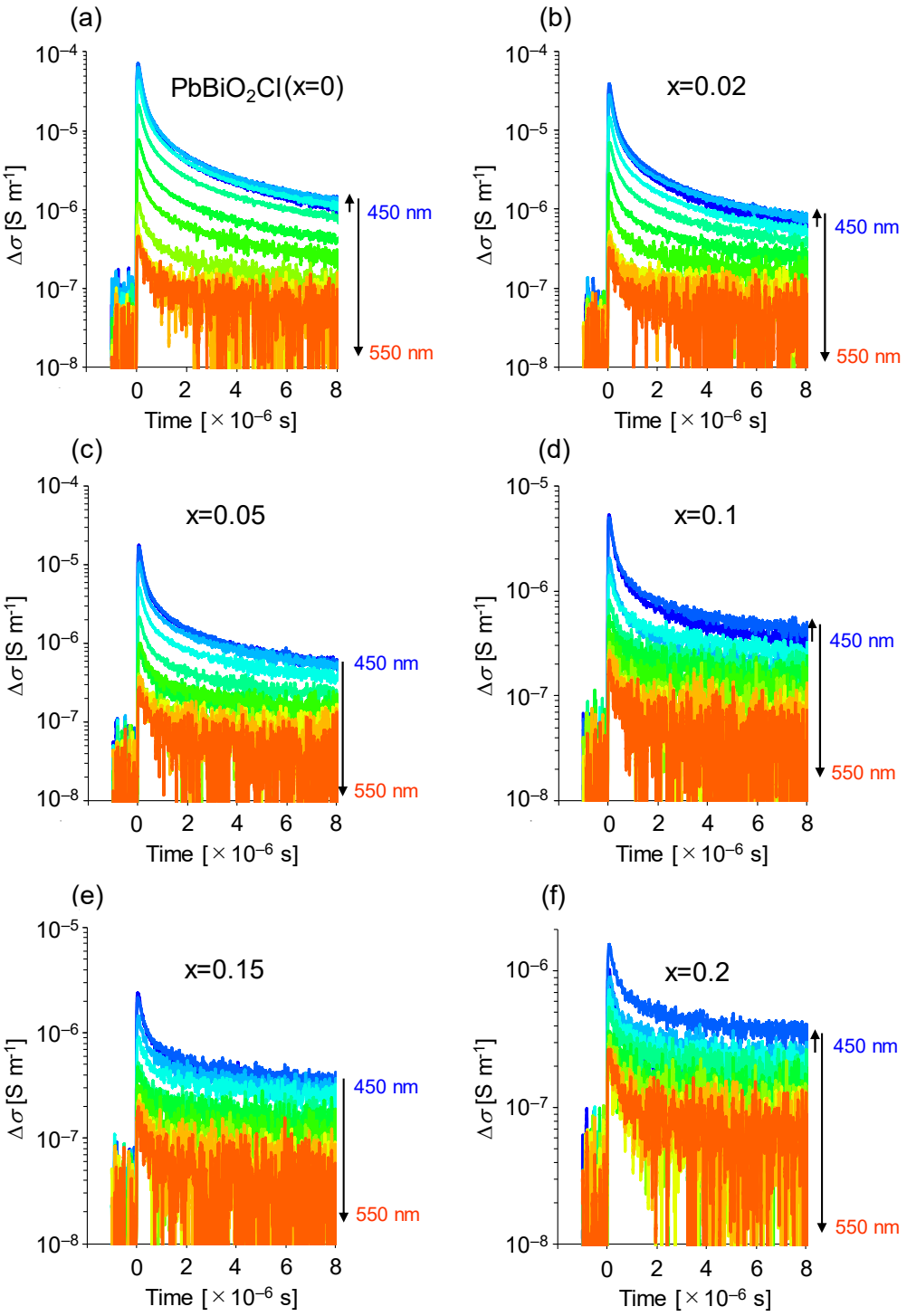

Figure S12. Photoconductivity transients: $\Delta\sigma(\lambda_{ex} = 450–550$ nm, $I_0 = 5.0\times10^{15}$ photons cm^{-2} per pulse^{-1}) of $Sr_xPb_{1-x}BiO_2Cl$ solid solutions (x = 0–0.2).

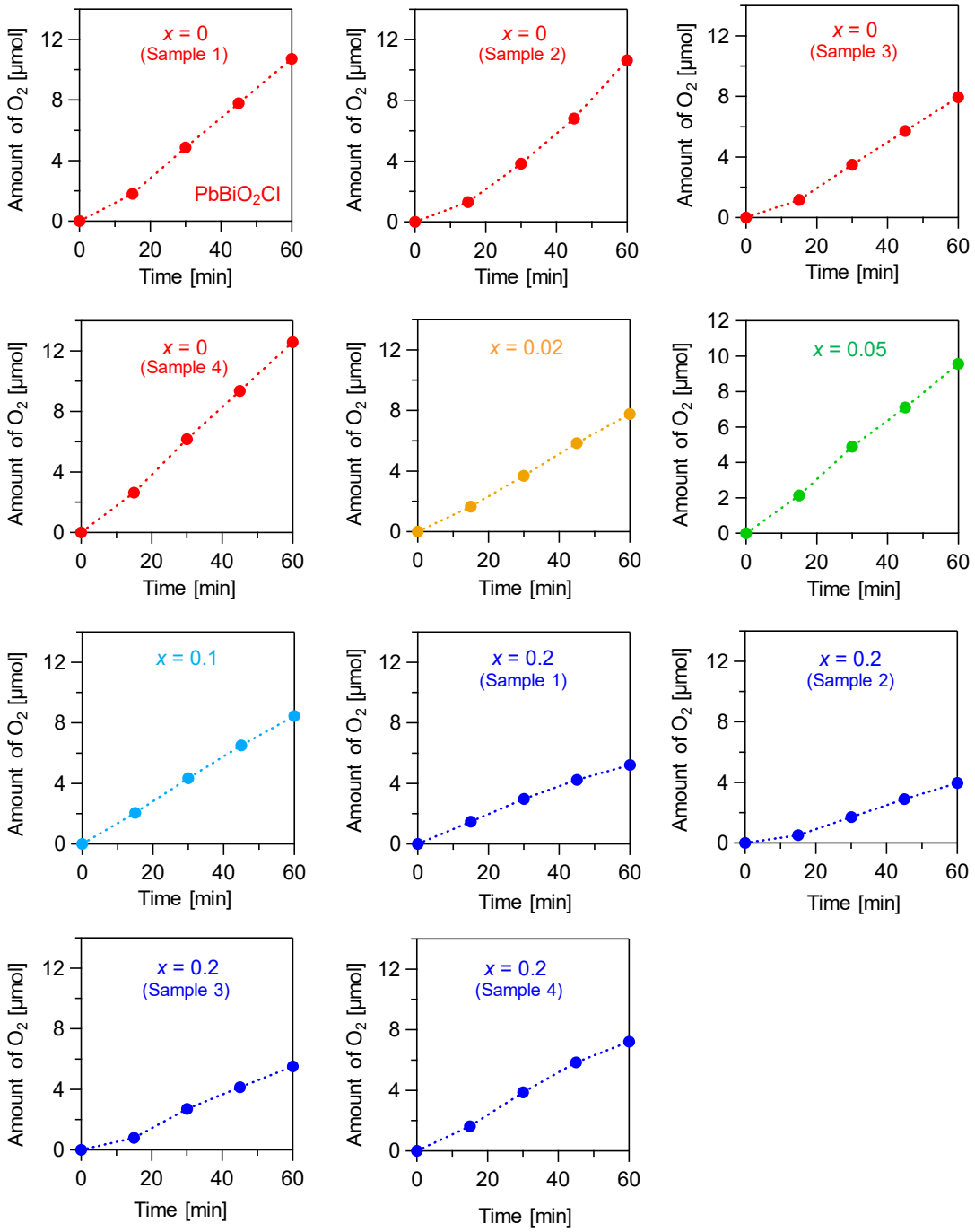

Figure S13. O_2 evolution over $Sr_xPb_{1-x}BiO_2Cl$ solid solutions (x = 0–0.2) in the presence of $AgNO_3$ under UV light (λ = 300–400 nm)

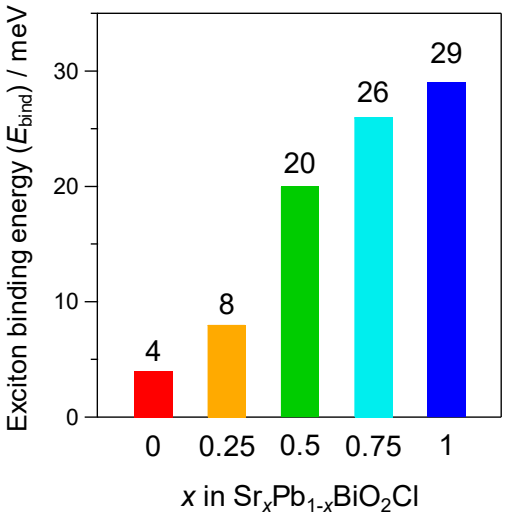

Figure S14. Calculated exciton binding energies of $Sr_xPb_{1-x}BiO_2Cl$.

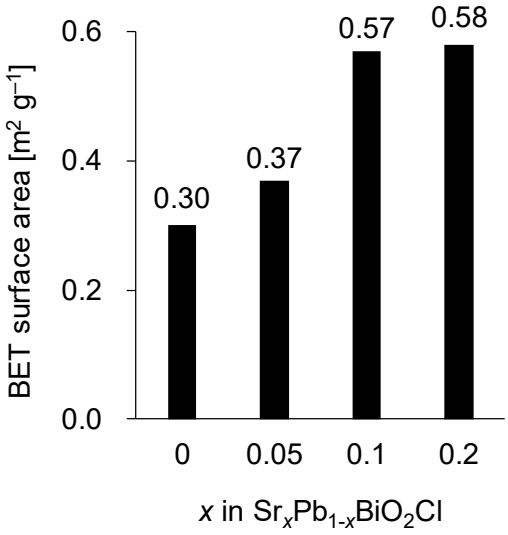

Figure S15. Specific surface area of $Sr_xPb_{1-x}BiO_2Cl$ solid solutions (x = 0–0.2)